Numerical Methods in Civil Engineering

Journal Homepage: https://nmce.kntu.ac.ir/

Reliability-based assessment of reinforced concrete columns under eccentric loads using refined first-order reliability method

Hossein Shahraki*, Ahmad Reyhani**

ARTICLE INFO

RESEARCH PAPER

Article history:
Received:
June 2022
Revised:
June 2023
Accepted:
February 2024

Keywords:
Reliability, RC column, Load eccentricity, Refined FORM, Cross-entropy optimization.

Abstract:

This paper presents an efficient approach for the failure probability assessment of reinforced concrete (RC) columns under the combination of gravity and seismic loads, considering the load's eccentricity. In the proposed approach, Limit State Functions (LSF) are conditionally formulated for the load eccentricity in the column, and the conditional reliability index is assessed using the Refined First-Order Reliability Method (R-FORM) based on the cross-entropy optimization method. The conditional reliability index and the probability density function of the load eccentricity have been used to estimate the failure probability of the column. The important feature of the proposed approach is a precise determination of the most probable failure point, which provides a precise estimation of the failure probability of the RC columns under different load eccentricities. The results indicate that the failure probability of the RC columns is sensitive to uncertainty in the load eccentricity and the structural system, mainly when the load eccentricity is in the tension failure region. The effect of longitudinal reinforcement varies depending on the probability density function of the load eccentricity and the region of the interaction diagram where the column is loaded.

1. Introduction

Reinforced concrete (RC) structures are widely used in Iran and almost worldwide. An RC structure's safety depends on its components' performance, especially columns [1]. Column's failure in an RC structure may lead to a catastrophic consequence. Therefore, it is necessary to measure the possibility of the failure occurrence quantitatively, considering the uncertainty associated with material properties, external load effects, and the relevant variables [2,3].

Structural reliability theory is a tool to bring the effect of uncertainty into the analysis procedure [4-6]. In this theory, the main goal is to find the probability of failure (P_f). This probability can be derived as:

$$P_f = P[LSF(\boldsymbol{X}) \le 0] = \int_{LSF \le 0} f(\boldsymbol{X})dx \qquad (1)$$

Where $f(\mathbf{X})$, is the joint probability density function of n-dimensional vector $\mathbf{X}$ of the basic random variables. Eq. (1) cannot be analytically assessed for most practical problems with high-dimensional random variables and complex forms of failure regions [7,8]. Consequently, different methods were proposed to estimate the probability of failure. Monte Carlo Simulation (MCS) is the most accurate method that can be used to solve probabilistic problems. However, it is not the most capable approach for time-consuming cases and problems with small probabilities because of its high computational costs [9]. Hence, many variance reduction and approximation methods, such as the First- and Second-order Reliability Methods (FORM and SORM) [10], stratified sampling [11], latin hypercube sampling [12], importance sampling [13], directional sampling [14], weighted average simulation [15], and subset simulation [16] have been developed to solve such problems. Since some simplifications and assumptions accompany the primary approach in these methods, they have some limitations compared to MCS. A novel method called Refined FORM (R-FORM) has been proposed that solves complex reliability problems efficiently with the appropriate

* *Corresponding author: Hossein Shahraki, Assistant Professor, Department of Civil Engineering, University of Bojnord, Bojnord, Iran. Email: h.shahraki@ub.ac.ir.*

** *Ahmad Reyhani, M.Sc. of Structural engineering, Department of civil Engineering, University of Bojnord, Bojnord, Iran. Email: a.reyhani@stu.ub.ac.ir.*

https://doi.org/10.52547/NMCE.2303.780

accuracy to overcome these limitations [17]. The main effort in this method is the precise search of the Most Probable Failure Point (MPFP) based on the Cross-Entropy Optimization (CEO) method.

Seismic hazards cause significant losses every year all over the world. For example, Yurdakul et al. [18] investigated the seismic damage and the social disruption observed after the Elazig-Sivrice earthquake in the non-structural and structural elements of the RC structures. Zafarani et al. [19] reported that numerous engineering structures collapsed or were considerably damaged in some regions under an intense earthquake in Iran.

To reduce the loss, better performance of the structure, especially columns, during intense earthquake action is desired. As one of the effective strategies, a lower target failure probability is proposed for RC columns in design codes (e.g., [20]) for the earthquake-dominated case. Generally, with the application of the design methods in codes, the target safety level can be achieved for RC columns. However, damage to RC columns subjected to a strong earthquake action is usually more severe than expected. Therefore, it is necessary to realistically determine uncertainties related to seismic loads to assess the failure probability of RC columns. For example, Jiang and Yang [21] considered the uncertainties associated with seismic loads based on a hypothetical model and then calculated the failure probability of the column. However, the precise estimation of the failure probability requires an accurate assessment of the seismic demands of RC columns in actual structures using Nonlinear Time History Analysis (NTHA).

This study focuses on the failure probability evaluation for the short columns designed according to Ref. [20]. The RC columns are usually subjected to axial compression and bending moment combinations. The failure probability evaluation of RC columns is a stochastic problem because of the inherent complexity in defining the Limit State Function (LSF), the interactive action between axial force and bending moment, and the lack of a closed-form solution to express resistance [23].

Baji and Ronagh [24] pointed out that the computed safety of a given column would depend on how the LSF was defined. The LSF based on axial load or bending moment criterion requires the safety assessment of the RC column based on system reliability or conditional probabilities, and their explicit formulation and implementation are difficult and complex for the whole column interaction curve; hence, many related studies [25-31] used criterion of the shortest load path from the initial loading in their study. It is possible to determine a unique quantity of axial force and bending moment for the whole interaction curve corresponding to that point, and the reliability index of the column can be calculated methodically using the criterion of the shortest load path.

When only the gravity loads act on the column, the applied axial force and bending moment are proportional to each other, and the load eccentricity keeps being fixed; thus, using the shortest load path method does not cause any problems [27-30]. However, for a column subjected to a horizontal load and a vertical load together (e.g., earthquake-dominated combination), because the horizontal load and vertical load both have a random property, the load eccentricity of RC columns under this combination is random, too. Therefore, the load eccentricity can be anywhere in the axial load and bending moment space, and it does not fall on a straight line with a specific eccentricity and leads to misleading reliability results [24, 32, 33]. The points mentioned above conclude that there may be significant errors in reliability results calculated with the fixed eccentricity criterion.

This study tries to propose an efficient approach for estimating the failure probability of the RC columns with high accuracy. To this end, LSF is conditionally formulated for the load eccentricity of the column, and the conditional reliability index is assessed using the R-FORM method. In R-FORM, the CEO method is used to determine the MPFP precisely. The conditional reliability index and the probability density function of the load eccentricity have been used to estimate the column failure probability. Similar formulation for different regions of column interaction diagram, realistic determination of uncertainties related to seismic loads of RC columns in different structural systems using NTHA, and considering the effect of random load eccentricity in failure probability assessment of the RC column are other advantages of the proposed approach.

2. Load model

The load model specified in Ref. [20] was used in the failure probability assessment of short RC columns. The factored load (U) was considered as follows:

$$U = max\begin{Bmatrix} 1.4D \\ 1.2D + 1.6L \\ 1.2D + L \pm E \\ 0.9D \pm E \end{Bmatrix} \quad (2)$$

D is the dead load, L is the live load, and E is the earthquake load.

It should be noted that various loads can exist in the load combinations accounted for in Ref. [20]. In this study, however, only the loads in Eq. (2) were considered for failure probability assessment. Dead load follows normal distribution with a bias factor (ratio of mean-to-nominal) and coefficient of variation (COV) of 1.05 and 0.10, respectively, while the 50-year maximum live load follows Extreme Type I distribution with a bias factor and COV of 1.0 and 0.25, respectively [2, 34]. The live axial load to dead axial load ratio and the live bending moment to dead bending

moment ratio are shown by η, which is assumed to be $\eta = 0.40$ in this study.

Column seismic load uncertainty depends on the site characteristics, structural system, cross-section, and reinforcement details. This study assesses the seismic loads based on NTHA using SAP2000. In NTHA, soil type and site characteristics should be considered in selecting records to resemble the site closely. To achieve this goal, the parameter of the average shear wave velocity in different layers up to the depth of 30 m from the base level ($\overline{v_s}$) is used. The studied structures are supposed to be on type III soil; according to Ref. [35], the average shear wave velocity for the selected records should be 175 to 375 m/s. Specifications of the selected records, including the magnitude (M_g), distance from the epicenter (R), and the average shear wave velocity, are shown in Table 1. The acceleration spectrum of the selected records for a damping ratio of 5% is given in Figure 1. In order to prevent dispersion in the results of NTHA, the selected records are scaled based on the design spectrum of Ref. [35]. The maximum seismic loads for records concerning the structural system, cross-sectional characteristics of the column, and reinforcement details are precisely extracted from SAP2000 to calculate the seismic load parameters of each column. The best distribution for maximum seismic loads is fitted based on the 20 records presented in Table 1. Accordingly, among the distribution functions that can describe the maximum seismic loads, extreme type I shows the best fit, so it is used to describe the maximum seismic loads of the column. The bias factor of the 50-year maximum seismic loads is considered 0.66 [36]. Table 2 lists the bias factor, COV, and type of distribution of loads.

Correlations between axial load and bending moment for dead, live and seismic loads, seismic axial load and dead axial load, seismic axial load and live axial load, seismic bending moment and dead bending moment, and seismic bending moment and live bending moment are considered with ρ. Jiang and Yang [21] stated that because statistical data for assessing the correlation of the load effects due to a load process are unavailable, the range from 0.23 to 0.33 is adopted as the correlation coefficient value. In this study, the values of the correlation coefficient close to the above range, i.e., $\rho = 0.20$ and $\rho = 0.40$, have been considered. In addition, $\rho = 0$ is also considered, showing the effect of the independence between the axial load and bending moment. Note that in the process of assessing the reliability of the RC columns, $\rho = 0$, $\rho = 0.20$, and $\rho = 0.40$ are denoted by $\rho 0$, $\rho 0.20$, and $\rho 0.40$, respectively.

3. Resistance model

For a short RC column with an eccentricity e along a fixed principal direction ($e = M/P$, M and P are the moment and the axial force, respectively) and a symmetrical section, its model for capacity calculation often adopts an Equivalent Rectangular Stress Block (ERSB) assumption in Ref. [20], as shown in Figure 2.

Based on the equilibrium of forces and strain compatibility, the resistance formulas of the RC column are given as

$$P = 0.85 f_c' ba + \sum_{i=1}^{n} f_{si} A_{si} \tag{3}$$

$$M = 0.85 f_c' ba\left(\frac{h}{2} - \frac{a}{2}\right) + \sum_{i=1}^{n} f_{si} A_{si}\left(\frac{h}{2} - d_i\right) \tag{4}$$

$$\begin{cases} -f_y \le f_{si} = E\varepsilon_{cu}\left(1 - \dfrac{d_i}{c}\right) \le f_y & d_i > a \\ -f_y \le f_{si} = \left[E\varepsilon_{cu}\left(1 - \dfrac{d_i}{c}\right)\right] - 0.85 f_c' \le f_y & d_i \le a \end{cases} \tag{5}$$

$$c = \frac{\varepsilon_{cu}}{\varepsilon_{cu} - \varepsilon_{s1}} d_1 \tag{6}$$

where $\alpha_1 f_c'$ is the concrete stress that is assumed to be uniformly distributed over an equivalent rectangular block with $\alpha_1 = 0.85$ and f_c' = concrete compressive strength; f_{si} is the stress in the ith layer of steel; f_y is the yield strength of steel; A_{si} is the area in the ith layer of steel; d_i is the depth in the ith layer of steel; h and b are the geometrical depth and section width, respectively; c is the depth of the neutral axis, and $a = \beta_1 c$ is the depth of ERSB; ε_{s1} and d_1 are the strain in the first layer of steel and the depth to that layer; $0.65 \le \beta_1 = 1.05\text{-}0.00714 f_c' \le 0.85$; $E_s = 200$ GPa is the elastic modulus of steel, and $\varepsilon_{cu} = 0.003$ is the assumed ultimate strain of concrete. Note that the neutral axis depth from Eq. (6) should be controlled by setting $\varepsilon_{s1} = Z\varepsilon_y$, where Z is an arbitrarily chosen value, and ε_y is the yield strain of steel. Positive values of Z correspond to compressive strains, and its negative values correspond to tensile strains.

Statistical data of variables required to define the column resistance is shown in Table 3. Dimensions of the column cross-section, as well as the elastic modulus of the steel, are treated as deterministic variables, since they affect the estimated failure probability insignificantly [23, 27, 37, 38]. For determining the distribution type of random variables, studies conducted by Ellingwood et al. [39] are considered. The bias factor and COV of f_c', f_y, and A_s are taken from Ref. [40].

Modeling error (B) is a factor for the resistance of the RC column, indicating ambiguities in the evaluation of P and M. According to Ref. [41], a normal probability distribution function (PDF) is used for B with a mean of 1.0 ($\mu_B = 1.0$) and a coefficient of variation of 0.065 ($COV_B = 0.065$) for the compression failure range and $\mu_B = 1.0$ and $COV_B = 0.03 + (0.065 - 0.03)\, e_b/e$ for the transition and tension failure ranges, where e_b represents the balanced eccentricity (See Figure 3).

Table 1: Specifications of 20 earthquake records used in NTHAs

NO	Earthquake	Year	Station	M_g	R (KM)	$\bar{v}_s$ 30 (m/s)
1	San Fernando	1971	LA - Hollywood Stor	6.61	22.77	316.46
2	Imperial Valley	1979	Delta	6.53	22.03	242.05
3	Imperial Valley-06	1979	El Centro Array #6	6.53	1.35	203.22
4	Imperial Valley-06	1979	Chihuahua	6.53	7.29	242.05
5	Superstition Hills	1987	El Centro Imp. Co	6.54	18.2	192.05
6	Superstition Hills-02	1987	Parachute Test Site	6.54	0.95	348.69
7	Loma Prieta	1989	Capitola	6.93	15.23	288.62
8	Loma Prieta	1989	Gilroy Array # 2	6.93	11.07	270.84
9	Golbaf	1989	Golbaf	5.90	0	320
10	Landers	1992	Coolwater	7.28	19.74	352.98
11	Landers	1992	Yermo Fire Station	7.28	23.62	353.63
12	Erzincan, Turkey	1992	Erzincan	6.69	4.38	352.05
13	Northridge	1994	Beverly Hills - Mughal	6.69	17.15	355.81
14	Northridge-01	1994	Northridge - Saticoy	6.69	12.09	280.86
15	Kobe, Japan	1995	Shin-Osaka	6.90	19.15	256
16	Chi-Chi, Taiwan	1999	CHY101	7.62	9.94	258.89
17	Duce, Turkey	1999	Bolu	7.14	12.04	293.57
18	Kocaeli, Turke	1999	Yarimca	7.51	4.83	297
19	Parkfield-02, CA	2004	Parkfield - Fault Zone 14	6.00	8.81	246.07
20	Bojnord	2017	Garmkhan	5.80	27	318

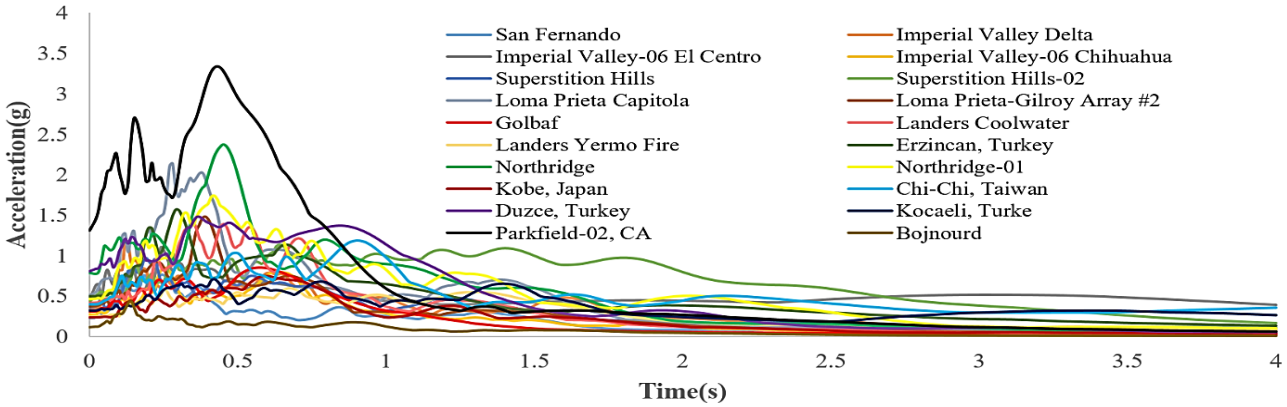

Fig. 1: Acceleration response spectra of the selected records for the 5% damping ratio

Table 2: Statistical data of load variables

Variable	Distribution	Bias factor	COV
Dead load	Normal	1.05	0.10
Live load	Extreme type I	1.00	0.25
Earthquake	Extreme type I	0.66	0.56

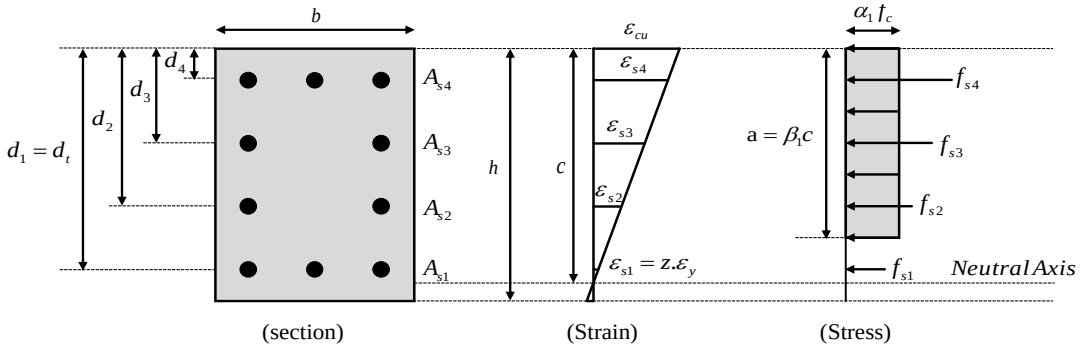

Fig. 2: Capacity model of the RC short columns

Table 3: Statistical data of resistance variables

Variable	Distribution	Bias factor	COV
f_c'=25 MPa	Normal	1.27	0.16
f_y=400 MPa	Log-normal	1.13	0.03
A_s	Normal	1.00	0.015
E_s	Deterministic	1.00	-
b	Deterministic	1.00	-
h	Deterministic	1.00	-
d	Deterministic	1.00	-

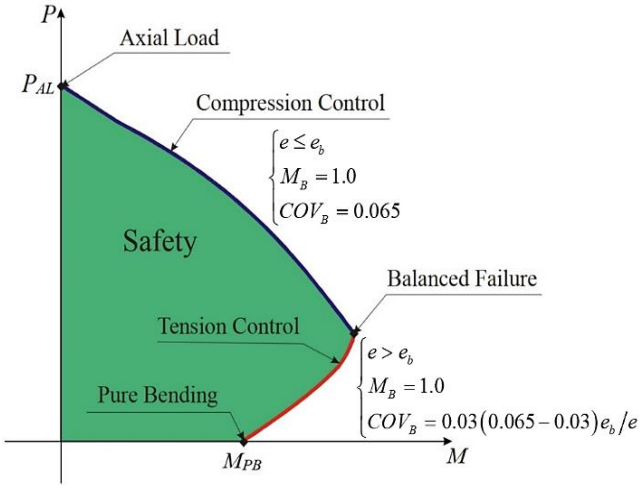

Fig. 3: Modeling error for the RC columns

4. Proposed approach for reliability assessment

According to [20], the combined nominal axial force and bending moment strength (P_n, M_n) of a column, multiplied by the strength reduction factor (φ), must be at least equal to the expected strength in order to obtain the design strength (P_R, M_R)

$$(P_R = \varphi P_n,\ M_R = \varphi M_n) \geq (P_u, M_u) \quad (7)$$

The expected strength (P_u, M_u) results from Eq. (2) and defines the maximum factorized load effect. The resistance reduction factors for the compression-controlled and tension-controlled behavior are 0.65 and 0.90, respectively. For the transition region, a linear interpolation between 0.002 and 0.005 strains can be made, which separates the compression and tension-controlled regions.

The LSF for an RC column can be defined based on three criteria: axial load, bending moment, and shortest load path from unloading conditions (See Figure 4). LSF based on the criteria of axial load and bending moment requires performing a safety assessment of the RC column based on a systemic approach, the explicit formulation and implementation of which is difficult and complex for the whole interaction diagram. To master these challenges, LSF is conditioned for eccentricity (e) as follows:

$$LSF = 1.0 - \left[\frac{\sqrt{(P_Q)^2 + (\frac{M_Q}{h})^2}}{B\sqrt{(P_R)^2 + (\frac{M_R}{h})^2}}\right]_e \quad (8)$$

where P_Q and M_Q are the axial force and the bending

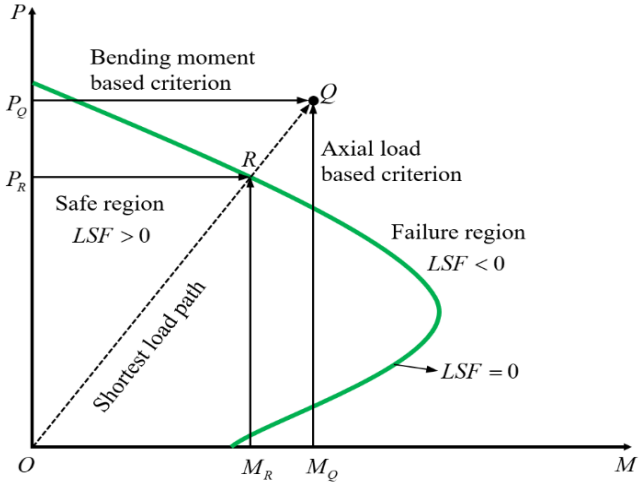

Fig. 4: Interaction diagram and criteria for selecting LSF

moment due to the random loads, respectively. The column resistance and loads for a given eccentricity value are calculated in the above formulation according to the column interaction diagram. According to Figure 4, $LSF < 0$ denotes the failure region, and $LSF > 0$ also indicates the safe region.

The definition of safety can be expressed in terms of failure probability P_f or reliability index β [8]. Structural reliability analysis aims to assess P_f for a given design procedure quantitatively, knowing the uncertainties associated with relevant parameters. FORM is widely used to estimate P_f due to the excellent balance between accuracy and efficiency for the reliability analysis by searching MPFP on the limit state surface [42]. However, finding MPFP and computing reliability index in the case of limit states with multiple MPFP or high nonlinearity is still a major significant challenge in this method [43, 44]. This paper employs an efficient algorithm (R-FORM) to search MPFP based on Ref. [17] with accurate results for highly nonlinear LSFs. In the R-FORM algorithm, it is assumed that the MPFP is on the LSF in the failure domain when the PDF of the basic random variables is maximized based on the following probabilistic optimization model:

$$Maximize \prod_{i=1}^{n} PDF_i$$
$$sub.to\ LSF(T^{-1}(\boldsymbol{Y})) \leq 0 \quad (9)$$

where PDF_i is the probability density function of the ith basic random variable; $\mathbf{Y} = (Y_1, Y_2, \cdots, Y_n)^T$ is the standard normal variable vector, and T^{-1} is a function that transforms the random variables in **Y**-space (standard normal variables) to **X**-space (the basic random variable).

The penalty approach solves the optimization problem in Eq. (9) [17]. The solution of the optimization problem in Eq. (9) is equivalent to solving the equation as follows:

$$Maximize\ \prod_{i=1}^{n} PDF_i(\boldsymbol{X}) - \lambda\xi\{LSF(\boldsymbol{X})\} \quad (10)$$

Where λ is defined as the penalty factor and $\xi\{LSF(\mathbf{X})\}$ is the penalty function, which is defined as $\min\left\{0, LSF\left(T^{-1}(\mathbf{Y})\right)\right\}$.

To find the MPFP using the probabilistic optimization model in Eq. (10), Consider a function S(**t**) over a search space $\Omega_{\mathbf{t}}$ with a single minimizer, $\mathbf{t}^* = \left[t_1^*, ..., t_n^*\right]^T \in \Omega_{\mathbf{t}}$, and the corresponding minimum γ^*:

$$S(\boldsymbol{t}^*) = \gamma^* = \min_{\boldsymbol{t} \in \Omega_t} S(\boldsymbol{t}) \quad (11)$$

We can now associate with the above optimization problem the estimation of the probability P_f = P(S(**t**) ≤ 0) using the CEO method, where t has the PDF. The adaptive CE method was developed for rare-event probabilities and combinatorial optimization; hence, the CE approach can be used to find an importance sampling distribution that concentrates all its mass in a neighborhood of the point $\mathbf{t}^*$. Sampling from such a distribution thus generates optimal or almost optimal states. The CE generates a sequence of statistical properties of the optimization model in order to update the probability distributions in each cycle according to the point mass at $\mathbf{t}^*$. This study implements the R-FORM algorithm to search MPFP based on the CEO method as specified in algorithm 1.

When implementing the CEO algorithm to search MPFP, the parameters of the CEO method are specified as follows [17]:

Algorithm 1: The R-FORM algorithm to search MPP based on the CEO method

- ✓ lower (X_{lb}) and upper bound (X_{ub}) of random variables
- ✓ number of samples (N_s)
- ✓ number of effective samples (N_{as})
- ✓ penalty factor (λ)

Data: LSF(**X**), probability density function of random variables, parameters of CEO method

1. Generate the random variables

for $\rightarrow 1 \le j \le N_s$

$\mathbf{X}(j) = \boldsymbol{X}_{lb}$ − (random number) * $(\boldsymbol{X}_{ub} - \boldsymbol{X}_{lb})$, end

2. Evaluate the probabilistic model

for $\rightarrow 1 \le j \le N_s$

$$F(j) = \prod_{i=1}^{n} \mathrm{PDF}_i\left[\mathbf{X}(j)\right] - \lambda \underbrace{\xi\left\{LSF\left[\mathbf{X}(j)\right]\right\}}_{\min\left\{0, LSF\left(T^{-1}(\mathbf{Y}j)\right)\right\}}$$, end

3. Determine the N_{as}

4. Compute means (μ_x) and standard deviations (σ_x) according to the N_{as} best fitness.

5. Generate the random variables with normal PDF

for $\rightarrow 1 \le j \le N_s$

$\mathbf{X}(j)$ = normal random number with a mean of μ_x and standard deviation of σ_x, end

6. Check whether μ_x and σ_x have stabilized; if not, $\lambda = 2\lambda$ and go to step 2.

7. Compute X_{best} and U_{best}

8. Compute the reliability index as $\beta_{ci} = \|U_{best}\|$

9. Compute $P_{f_{ci}} = \Phi(-\beta_{ci})$

The general framework of the proposed approach to assessing the P_f of the short RC column is shown in Figure 5, where *D*, *L* and *E* subscripts correspond to dead, live, and seismic loads, respectively, μ and σ are mean. The standard deviation of random variables, respectively, e_{1i} is the load eccentricity based on the dominant load combination, and e_{2i} is the eccentricity corresponding to Z_i based on the interaction diagram.

It should be noted that β_{ci}, and $f(e_i)$ are the reliability index and the probability density function corresponding to e_i, respectively. The codes of the proposed approach are written in MATLAB.

5. Description of structures and modeling details

In this study, three RC structures, including a 2-story moment frame (F1 structure), a 4-story moment frame (F2 structure), and a 4-story frame consisting of a moment frame and RC shear wall (F3 structure), were designed following Ref. [20] based on intermediate ductility criteria, are investigated. These structures have been selected to meet the short-column criterion based on Ref. [20]. The structures have three bays with the same length of 4 m, and the height of each floor is 2.6 m. Specifications of columns and beams in the investigated structures are shown in Figs. 6 and 7.

The studied structures were modeled in SAP2000 under a dead load of 2400 kg/m and a live load of 800 kg/m uniformly distributed on all floors, and then the direct-integration NTHAs were performed under the selected records. Beam and column elements were modeled as nonlinear frame elements with plastic hinges (PM2M3 for columns and M3 for beams) at both ends. The procedure has been implemented using the default hinge properties based on ASCE 41-17 [44] since the cross-section, reinforcement content, and loads on them were precisely modeled. The plastic hinge length was assumed to be half the member depth for all section types, typically used for RC sections [45]. Nonlinear fiber elements were used throughout the length of RC shear walls, and Mander's stress-strain model and the bilinear elastoplastic model were considered for concrete and steel fibers, respectively. It has been assumed that the out-of-place actions in shear walls remain elastic, and the inelastic action was modeled only in the in-place direction. The interaction of moment and axial loading in the

shear wall was modeled using the interacting P-M3 fiber hinges. The pivot hysteresis type was assigned to all hinges for nonlinear concrete hysteretic behavior.

6. Results and discussions

In this study, P_f is assessed for 8 columns subjected to various eccentricities whose details are illustrated in Table 4. The safety of the studied columns is evaluated based on the proposed approach, using statistical data provided for resistance and loads in Tables 2 and 3. It can also be noted that $e_0 = 350$ mm is used to normalize the load eccentricity, an arbitrarily chosen value. A simple Monte Carlo Simulation (MCS) is used to estimate β_{c_i} of the C12 column under several eccentricities. To verify the accuracy of the results obtained by the proposed approach, shown in Table 5. The number of simulation cycles for each eccentricity is 10^6, and the values in parentheses indicate the relative errors (%). Table 5 suggests that the results obtained using the proposed approach agree with the values obtained from MCS.

In Fig. 8, the P_f of columns is compared in the studied structure for ρ0.40. Numerical results show that the P_f of the RC columns is sensitive to seismic loads applied to them. Based on the results, in the F1 structure, due to the increased axial load and seismic bending moment on the C12 column compared to the C16 column by 41.42% and 93.36%, respectively, the C12 column has greater P_f for high eccentricities ($e > 0.80e_0$). However, in low eccentricities ($e \leq 0.80e_0$), P_f variations of the C12 and C16 columns are insignificant relative to each other under the dominated load combinations (see Fig. 8-a).

In the F2 structure, due to the simultaneous action of significant axial force and bending moment in the C21 column, P_f of this column at high eccentricities ($e > 1.0e_0$) is higher than the C22 column. However, in low eccentricities ($e \leq 1.0e_0$), P_f for C21 and C22 columns are very close (see Fig. 8-b). According to Fig. 8-c, on the second floor of the F2 structure, due to the reduced axial load and seismic bending moment by 27.43% and 51.51%, respectively, the C25 column has less P_f at various eccentricities compared to the C21 column.

A comparison of the C29 and C25 columns on the second and third floors of the F2 structure reveals that the C29 column, due to the reduction of axial load and seismic bending moment by 40.32% and 36.61%, respectively, has less P_f for $e > 1.80e_0$. Nonetheless, in the load eccentricities range of $e \leq 1.80e_0$, P_f in the C29 column is upper due to decreased cross-sectional capacity and consequently increasing the difference between the point corresponding to the load and resistance in the standard normal space. Similarly, due to the lower axial load and seismic bending moment applied to the C29 column compared to the C21

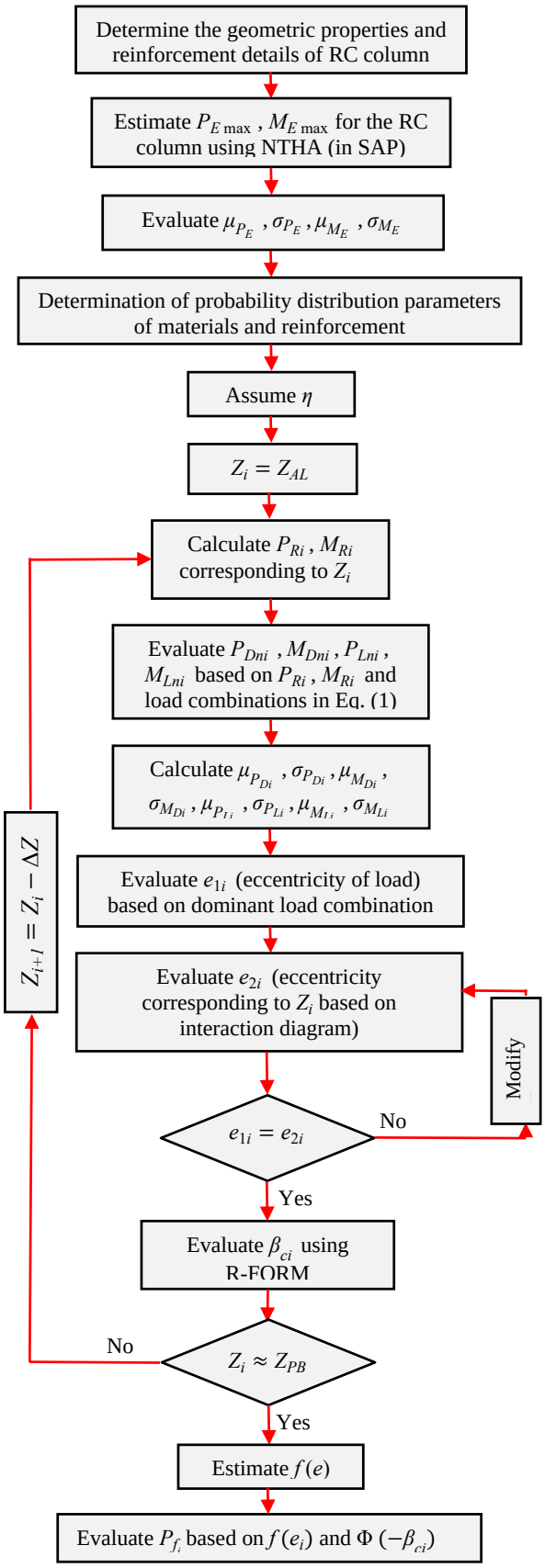

Fig. 5: Framework of the proposed approach to assessing the P_f of the RC columns.

column by 56.69% and 69.27%, respectively, the C29 column has lower P_f in the range of $e > 1.30e_0$. But in the load eccentricity range of $e \leq 1.30e_0$, P_f in the C29 column

is upper due to decreased cross-sectional capacity (see Fig. 8-c). By comparing the graphs in Fig. 8-c, we can conclude that the highest value of P_f is that of the C29 column when compared with the other columns, whereas the lowest was for the C25 column. In addition, the C21 column also has the highest values of P_f at high eccentricities.

Consider the side columns of C21 in the F2 structure by RC moment frame and C31 in the F3 structure consisting of RC moment frame and RC shear wall. Although in the C31 column, the longitudinal reinforcement ratio and the cross-sectional dimensions are decreased by 15.31% and 12.5%, respectively, P_f variations of the C21 and C31 columns are insignificant relative to each other at low eccentricities ($e < 0.90e_0$). However, for $e \geq 0.90e_0$, P_f of the C31 column is less due to a significant reduction of axial load and seismic bending moment due to the RC shear wall in the F3 structure (Fig. 8-d)

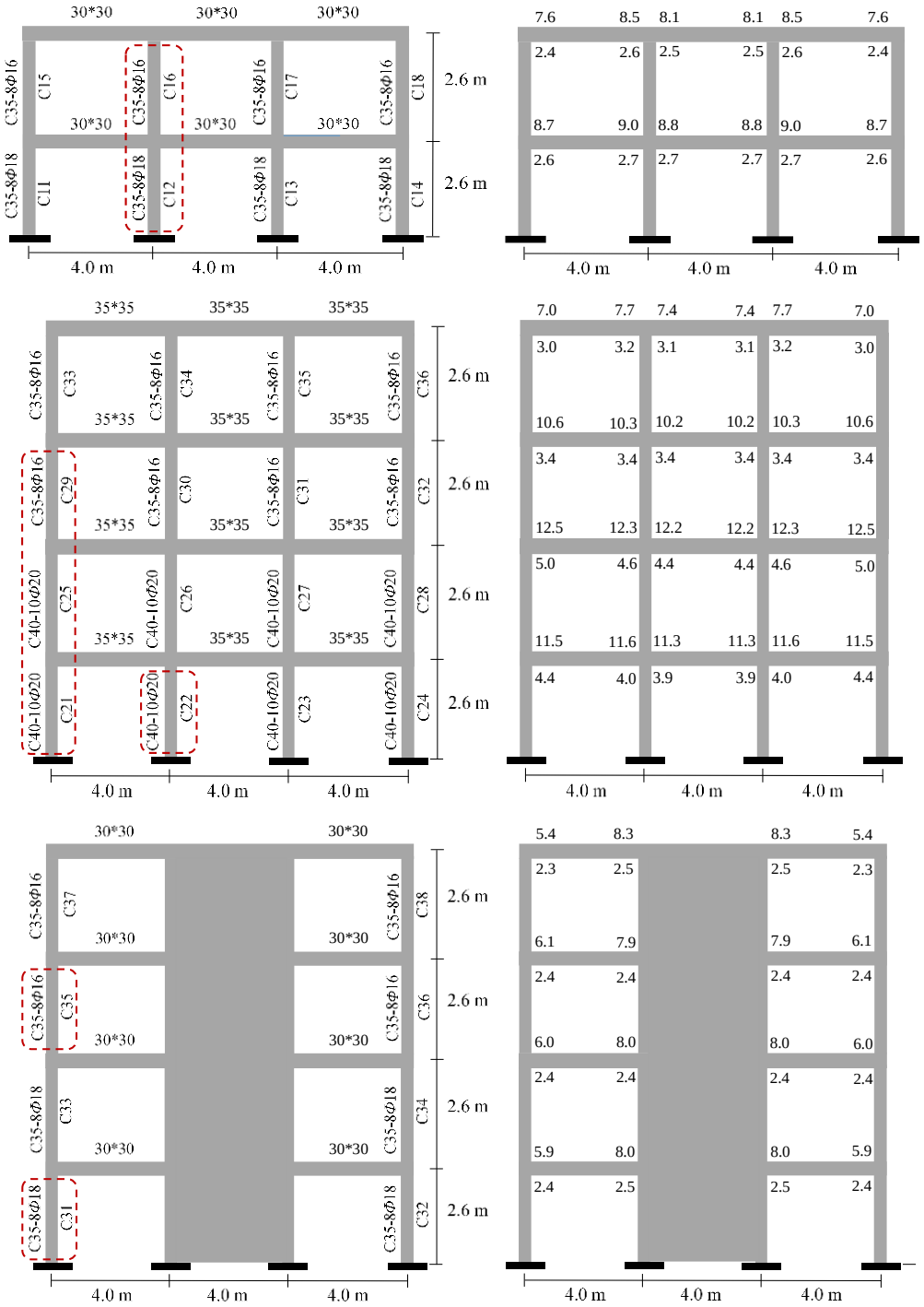

Fig. 6: Structural sections and longitudinal reinforcement of beams in F1, F2, and F3 structures

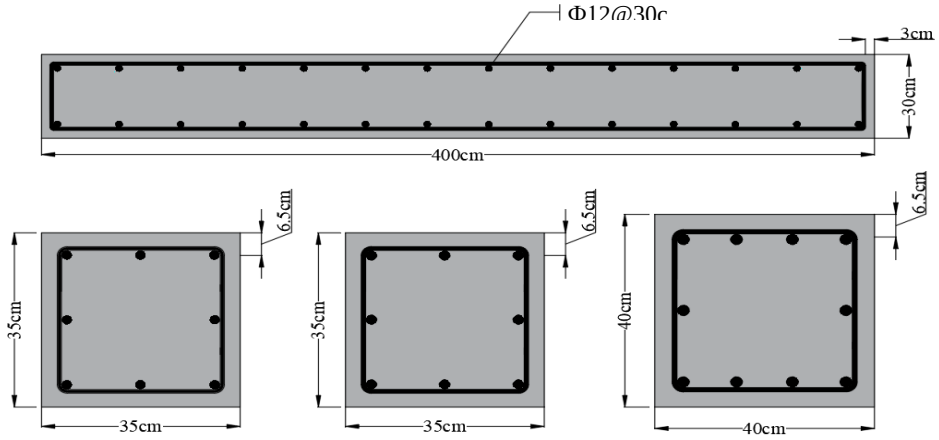

Fig. 7: Cross section and reinforcement details of columns and shear wall

Table 4: Columns selected for P_f assessment

Column	Cross Section	Reinforcement Ratio (ρrr %)	$P_{E\,max}$ (KN)	$M_{E\,max}$ (KN.m)
C12	C35-8Φ18	1.66	3.8351	162.25
C16	C35-8Φ16	1.31	2.7119	83.912
C21	C40-10Φ20	1.96	185.32	268.49
C22	C40-10Φ20	1.96	10.496	308.72
C25	C40-10Φ20	1.96	134.49	130.18
C29	C35-8Φ16	1.31	80.263	82.516
C31	C35-8Φ18	1.66	46.595	84.221
C35	C35-8Φ16	1.31	23.889	9.46

Table 5: Comparison of $\beta_{ce_i\,(\text{R-FORM})}$ and $\beta_{ce_i\,(\text{MCS})}$ for C12 column

e/e_0	$\beta_{ci\,(\text{R-FORM})}$	$\beta_{ci\,(\text{MCS})}$
0.042	4.1999 (0.041)	4.1982
0.072	4.2170 (0.156)	4.2236
0.332	3.9325 (0.617)	3.9084
0.495	3.1793 (0.617)	3.1598
0.693	2.4487 (0.815)	2.4289
1.833	1.5251 (1.006)	1.5406
2.133	1.4629 (0.537)	1.4708
3.783	1.3246 (1.164)	1.3402

In the C29 column of the structure with moment frame compared to the C35 column in the structure consisting of RC moment frame and RC shear wall, as shown in Fig. 8-e, P_f highly increased due to the increased seismic loads for $e \geq 0.97e_0$. At low eccentricities ($e \leq 0.79e_0$), P_f of C29 and C35 columns are very close to each other, whereas in the range of $0.79 < e < 0.97e_0$, P_f of the C35 column is higher due to the gravity-dominated load combination. In the F3 structure, although the longitudinal reinforcement ratio of the C31 column on the first floor is 26.72% greater than the C35 column on the third floor, because of the higher seismic loads applied to the C31 column, P_f of the C31 column in high eccentricities ($e \geq 1.05e_0$) is increased due to the seismic-dominated load combination. However, for $e < 1.05e_0$, P_f of the C35 column is upper than the C31 column due to the gravity-dominated load combination (Fig. 8-f).

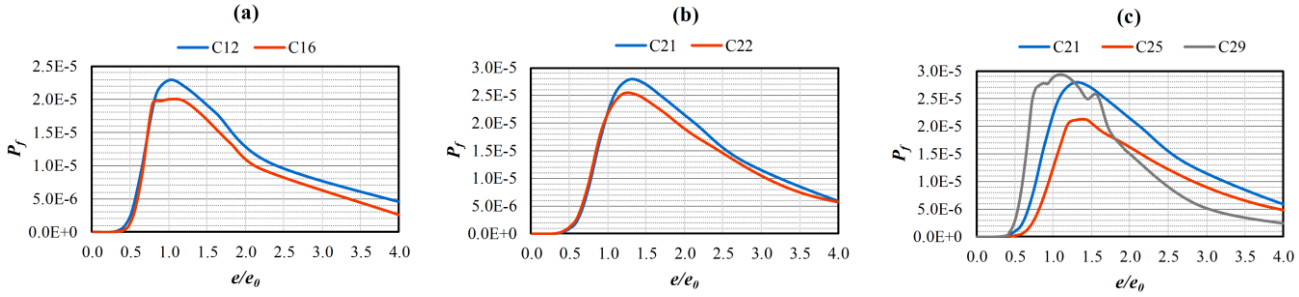

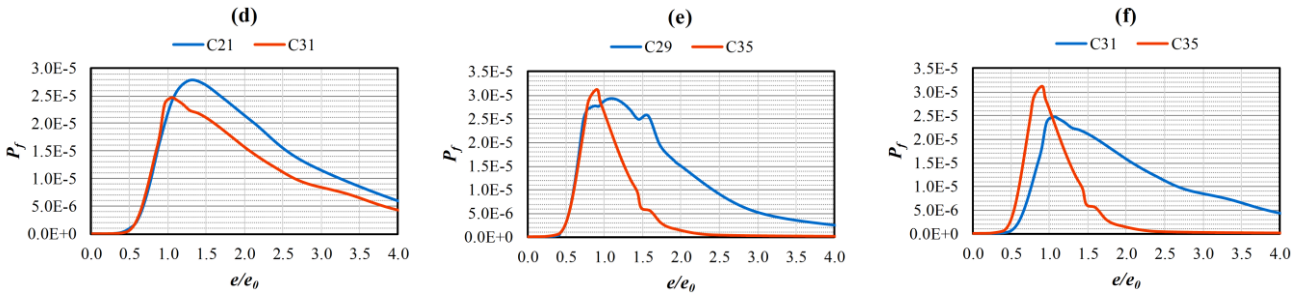

Fig. 8: Variation P_f versus load eccentricity for η=0.40 and ρ0.40

The results in Fig. 9 show that the P_f of the RC columns, in many cases, is sensitive to ρ. In the compression failure region ($e \leq e_b$), the effect of ρ on P_f of the RC columns is insignificant, but in the tension failure region ($e > e_b$), ρ significantly influences P_f in most of the columns. As can be seen in Fig. 9, $P_{f_{max}}$ of the RC short columns happens in the range of e_b/e_0 to $e/e_0 = 1.50$ for ρ0, ρ0.20 and ρ0.40.

The results reveal that as ρ increases, P_f of the columns designed close to the balanced point decreases (C12 and C22 columns); nevertheless, P_f of the columns designed in both regions of the compression and tension failure increases as ρ increases (C16, C21, C25, C29, C31, and C35 columns), consequently, ignoring ρ can underestimate or overestimate P_f of the RC short columns.

As shown in Fig. 9, the P_f of the RC column in the compression failure is much lower than the tension failure, which arises from the design requirements. As previously mentioned, the strength reduction factor, φ, is 0.65 for the compression failures because the RC column will fail suddenly without warning, although $\varphi = 0.90$ for the tension failure, which is accompanied by large deformations and warning before collapse. Furthermore, P_R and M_R of the RC column decrease in the tension failures as eccentricity increases; subsequently, the P_f of the RC column will be lower in the compression failures than in the tension failures. Generally, target safety levels for structural members are set based on experience with the performance of existing structures, consequences of member failures, and construction cost. For an RC column designed with 50 years of service life, the target failure probability is selected equal to 3.1671×10^{-5} (β = 4.0) for both tension failures and compression failures (see Refs. [9,21]). The results of the proposed approach indicate that P_f s of the studied columns are less than the target failure probability for both tension failure and compression failures (see Fig. 9). Thus, the design requirements of Ref. [20], such as the longitudinal reinforcement ratio and code-based factors, provide an appropriate safety level for the RC short columns.

To investigate the effect of longitudinal reinforcement ratio (ρrr) on P_f, the C12 column is selected as a model, and P_f is evaluated for ρrr =1.66%, ρrr =2.95%, ρrr =4% by considering ρ0, ρ0.20 and ρ0.40 (see Fig. 10). As illustrated in Fig. 10, for low eccentricities, P_f of the column by ρrr = 2.95% is lower than the other cases, and the column with ρrr = 1.66% has the maximum P_f. In the column by ρrr = 4.0%, as the load eccentricity increases, the effect of reinforcing steel in the resistance of the column increases, so the P_f s of this column are lower than the other cases. On the other hand, in the high eccentricities, the P_f of the column by ρrr = 2.95 % is higher than the other cases due to the significant seismic bending moment applied to the column derived from the NTHA of the structure.

7. Conclusion

The main contribution of this study is to develop an efficient approach to assess the reliability of reinforced concrete (RC) columns under a combination of gravity and seismic loads, considering uncertainty in the load eccentricity. For this purpose, Limit State Function (LSF) is defined based on the conditional axial force and bending moment for each possible eccentricity on the interaction diagram. Then, using the refined FORM, which employs the cross-entropy optimization (CEO) method to find the most probable failure point (MPFP), the conditional reliability index of RC columns is estimated in two different structural systems, and the failure probability of RC column is assessed based on the conditional reliability index along with the probability density function of the load eccentricity. A comparison of the results derived from R-FORM and MCS (with 10^6 simulations) demonstrated that the relative error is smaller than 1.2% for eccentricities corresponding to compressive, balance, and tensile failures; subsequently,

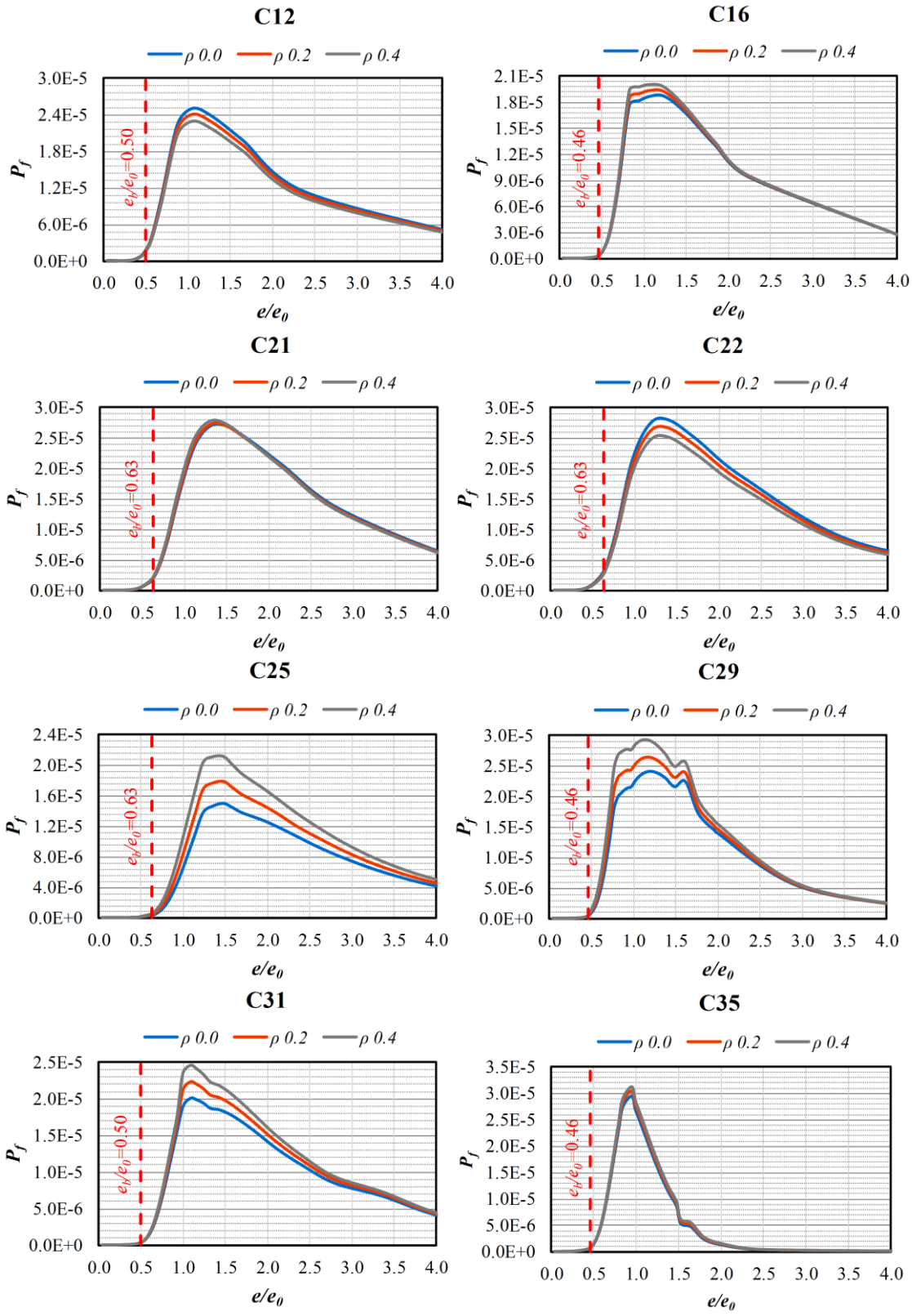

Fig. 9: Effect ρ on P_f in columns for η = 0.40

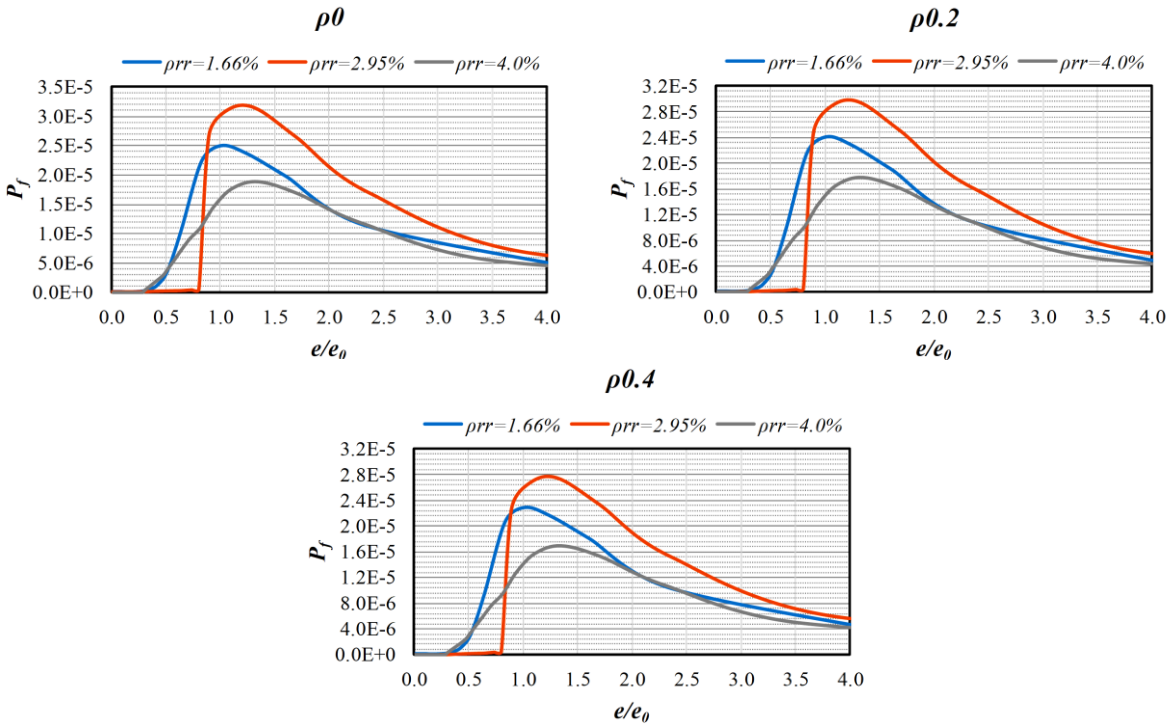

Fig. 10 Effect ρrr on P_f of C12 column for η = 0.40

R-FORM provides a precise evaluation of the reliability of RC columns under different load eccentricities. In addition, it is found that the failure probability of the RC columns is sensitive to the uncertainty in the load eccentricity, mainly when the load eccentricity is in the tension failure region. The failure probability of the column may be underestimated or overestimated, ignoring the uncertainty in the load eccentricity.

The lowest failure probability was obtained for low eccentricities in the compression failure region; failure probability was significantly increased for the transition region of the column interaction diagram. Our reviews showed that the reliability level associated with the tension failure region is lower than that associated with the compression failure region. The cause of such a trend may be attributed to the characteristics of the tension failure region, including the more significant strength reduction factor, the higher location of the neutral axis, and more significant bending effects compared to the compression failure region.

The amount of longitudinal steel has a significant effect on the failure probability of the column. The findings in this study show that in actual structures, the failure probability of the RC columns with different reinforcement ratios depends on both the resistance and variations in seismic demands derived from the structure's NTHA. However, in the tension failure region, the RC column with the highest reinforcement ratio had the highest safety indices among all reinforcement ratios.

The investigation of the failure probability for the RC columns in the structures with the moment-resisting frame and the structure consisting of the moment-resisting frame and RC shear wall revealed that the failure probability is sensitive to the type of structural system and the position of the column in the structure. In addition, it is found that in the tension failure region, the RC shear wall plays a vital role in reducing the failure probability or improving the reliability of the column under seismic excitation.

Finally, it is proved that the design requirements of ACI, such as the longitudinal reinforcement ratio and the code-based factors, provide the expected level of safety (β = 4.0) for the short RC columns when random properties of resistance and the load eccentricity are modeled.

References:

[1] Shahraki, H., Shabakhty, N. (2015). THE SEISMIC PERFORMANCE RELIABILITY OF REINFORCED CONCRETE MOMENT STRUCTURES. Tehnicki vjesnik/Technical Gazette, 22(1), 151-160, https://doi.org/10.17559/TV-20140330122450.

[2] Wang C (2021) Structural Reliability and Time-Dependent Reliability. Springer Nature, Switzerland.

[3] Kim JH, Lee SH, Paik I, Lee HS (2015) Reliability assessment of reinforced concrete columns based on the P-M interaction diagram using AFOSM. Structural Safety 55: 70-79.

[4] Li G, Meng Z, Hu H (2015) An adaptive hybrid approach for reliability-based design optimization. Structural and Multidisciplinary Optimization 51:1051-1065.

[5] Tuken A, Dahesh MA, Siddiqui NA (2017) Reliability assessment of RC shear wall-frame buildings subjected to seismic loading. Computers and Concrete 20: 719- 729.

[6] Kamel A, Dammak K, Yangui M, El Hami A, Ben Jdidia M, Hammami L, Haddar M (2021) A Reliability optimization of a coupled soil structure interaction applied to an offshore wind turbine. Applied Ocean Research 113: 102641.

[7] Kazemi Elaki N, Shabakhty N, Abbasi Kia M, Sanayee Moghaddam S (2016). Structural reliability: an assessment using a new and efficient two-phase method based on artificial neural network and a harmony search algorithm. Civil Engineering Infrastructures Journal 49: 1-20.

[8] Nowak A S, Iatsko O (2020) Load and resistance factors for prestressed concrete girder bridges. Budownictwo i Architektura 19: 103-115.

[9] Rubinstein RY, Kroese DP (2017) Simulation and the Monte Carlo Methods, 3rd edn. John Wiley & Sons, New Jersey.

[10] Nguyen H L, Tran V T, Pham Q T (2019) Reliability-based analysis of machine structure using second-order reliability method. Journal of Advanced Mechanical Design, Systems, and Manufacturing 13: JAMDSM0063-JAMDSM0063.

[11] Shields MD, Teferra K, Hapij A, Daddazio RP (2015) Refined stratified sampling for efficient Monte Carlo-based uncertainty quantification. Reliability Engineering & System Safety 142:310-325.

[12] Olsson A, Sandberg G, Dahlblom O (2003) On Latin hypercube sampling for structural reliability analysis. Structural Safety 25:47-68.

[13] Papaioannou I, Papadimitriou C, Straub D (2016) Sequential importance sampling for structural reliability analysis. Structural Safety 62:66-75.

[14] Shayanfar MA, Barkhordari MA, Barkhori M, Barkhori M (2018) An adaptive directional importance sampling method for structural reliability analysis. Structural Safety 70:14-20.

[15] Okasha NM (2016) An improved weighted average simulation approach for solving reliability-based analysis and design optimization problems. Structural Safety 60:47-55.

[16] Xiao S, Reuschen S, Köse G, Oladyshkin S, Nowak W (2019) Estimation of small failure probabilities based on thermodynamic integration and parallel tempering. Mechanical Systems and Signal Processing 133: 106248.

[17] Ghohani Arab H, Rashki M, Rostamian M, Ghavidel A, Shahraki H, Keshtegar B (2019) Refined first-order reliability method using cross-entropy optimization method. Engineering with Computers 35: 1507-1519, https://doi.org/10.1007/s00366-018-0680-9

[18] Yurdakul Ö, Duran B, Tunaboyu O, Avşar Ö (2021) Field reconnaissance on seismic performance of RC buildings after the January 24, 2020 Elazığ-Sivrice earthquake. Natural Hazards 105: 859-887.

[19] Zafarani H, Jafarian Y, Eskandarinejad A, Lashgari A, Soghrat M R, Sharafi H, Afraz M (2020) Seismic hazard analysis and local site effect of the 2017 Mw 7.3 Sarpol-e Zahab, Iran, earthquake. Natural Hazards 103: 1783-1805.

[20] ACI 318 Committee (2014) Building Code Requirements for Structural Concrete. American Concrete Institute: Farmington Hills, MI, USA.

[21] Jiang Y, Yang W (2013) An approach based on theorem of total probability for reliability analysis of RC columns with random eccentricity. Structural Safety 41: 37-46.

[22] Guérin M, Mohamed H M, Benmokrane B, Nanni A, Shield CK (2018) Eccentric Behavior of Full-Scale Reinforced Concrete Columns with Glass Fiber-Reinforced Polymer Bars and Ties. ACI Structural Journal 115: 489-499.

[23] Hong H, Zhou W (1999) Reliability Evaluation of RC Columns. Journal of Structural Engineering, ASCE 125: 784–790.

[24] Baji H, Ronagh H R (2012) Effect of relative intensity of wind load on the RC column reliability in tall buildings. The Structural Design of Tall and Special Buildings 21: 492-504.

[25] Israel M, Ellingwood B R, Corotis R (1987) Reliability-Based Code Formulations for Reinforced Concrete Buildings. Journal of Structural Engineering, ASCE 113: 2235-2252.

[26] Diniz SMC, and Frangopol D M (2003) Safety evaluation of slender high-strength concrete columns under sustained loads. Computers & Structures 81: 1475-1486.

[27] Szerszen MM, Szwed A, Nowak A S (2005) Reliability Analysis for Eccentrically Loaded Columns. ACI Structural Journal 102: 676-688.

[28] Baji H, Ronagh H R (2011) Effects of cross-sectional shape on the reliability of RC columns. Structural Concrete 12: 262-269.

[29] Wang N, Ellingwood B R (2015) Limit state design criteria for FRP strengthening of RC bridge components. Structural Safety 56: 1-8.

[30] Peng F, Xue W (2019) Reliability Analysis of Eccentrically Loaded Concrete Rectangular Columns Reinforced with Fiber-Reinforced Polymer Bars. ACI Structural Journal 116: 275-284.

[31] Reyhani A., Shahraki H. (2023) Parametric and sensitivity analysis in assessment the probabilistic vulnerability of RC short columns, MCEJ; 22 (1) :53-66, in Persian.

[32] Jiang Y, Zhou H, Beer M, Wang L, Zhang J, Zhao L (2017) Robustness of Load and Resistance Design Factors for RC Columns with Wind-Dominated Combination Considering Random Eccentricity. Journal of Structural Engineering, ASCE 143: 146– 159.

[33] Jiang Y, Peng S, Beer M, Wang L, Zhang J (2019) Reliability evaluation of reinforced concrete columns designed by Eurocode for wind-dominated combination considering random loads eccentricity. Advances in Structural Engineering 23: 146-159.

[34] Mahmoudkalayeh S, Mahsuli M (2021) Ramifications of blind adoption of load and resistance factors in building codes: reliability-based assessment. Bulletin of Earthquake Engineering 19: 963-986.

[35] BHRC (2014) Iranian Code of Practice for Seismic Resistant Design of Buildings. Building and Housing Research Center: Standard No. 2800, 4th ed., Tehran, Iran.

[36] Nowak A S, Rakoczy A M (2013) Uncertainties in the building process. Bulletin of the Polish Academy of Sciences: Technical Sciences 61: 129-135.

[37] Tang C H, Yang Y C (2011) Loading Correlation for Reliability Analysis of Reinforced Concrete Columns. Advanced Materials Research 243-249: 396-405.

[38] Floris, C., & Mazzucchelli, A. (1991) Reliability assessment
of RC column under stochastic stress. Journal of Structural Engineering, 117(11), 3274-3292.

[39] Ellingwood B R, Galambos T V, MacGregor J G, Cornell C (1980) Development of a probability based load criterion for American National Standard A58. NBS Special Publication 577, Washington, DC, USA.

[40] Nowak A S, Collins K R (2012) Reliability of Structures. CRC Press, New York.

[41] Mirza S A (1996) Reliability-based design of reinforced concrete columns. Structural Safety 18: 179-194.

[42] Goswami S, Ghosh S, Chakraborty S (2016) Reliability analysis of structures by iterative improved response surface method. Structural Safety 60: 56-66.

[43] Chau, M.Q., Han, X., Bai, Y.C. and Jiang, C. (2012). A Structural Reliability Analysis Method Based on Radial Basis Function, *Computers, Materials & Continua*, 27(2), 128-142.

[44] ASCE 41-17 (2017), Seismic Evaluation and Retrofit of Existing Buildings; American Society of Civil Engineers: Reston, VA, USA.

[45] Inel, M., & Ozmen, H. B. (2006), Effects of plastic hinge properties in nonlinear analysis of reinforced concrete buildings. *Engineering structures*, *28*(11), 1494-1502.